Reduction of Feasible Parameter Space of the Inverted Soil Hydraulic Parameter Sets for Kosugi Model

Joseph Alexander Paul Pollacco,[1] Paolo Nasta,[2] José M. Soria-Ugalde,[3] Rafael Angulo-Jaramillo,[4] Laurent Lassabatere,[4] Binayak P. Mohanty,[1] and Nunzio Romano,[2]

Abstract: Effective soil hydraulic parameters of soil vegetation atmosphere transfer (SVAT) models can be derived in a cost-efficient way by inverse modeling. Nevertheless, a serious drawback of SVAT models based on Richards' equation is that they require as many as five unexploited correlated hydraulic parameters. To reduce the feasible parameter space, we propose a method to prevent nonphysical combinations of soil hydraulic parameter sets obtained by optimization. We adopt the soil hydraulic analytical model by Kosugi because it enables the feasible parameter space to be reduced by predicting parameter σ from R_m, which are the variance and mean of the log-transformed soil pore radius, respectively. To further decrease the parameter space, we derive two models to predict saturated hydraulic conductivity, K_s, from three or four Kosugi soil water retention parameters, respectively. These two models are based on the combination of the Hagen-Poiseuille and Darcy equations that use three semiempirical parameters (τ_1, τ_2, and τ_3) calibrated on large UNSODA and HYPRES databases. Our derived models are compared with a version of the Mishra and Parker (1990. *Ground Water*. 28:775–777) K_s model being modified to account for the parameters of Kosugi's relationships. The results show that the uncertainties of the developed K_s model are comparable to the uncertainties of K_s measurements. Moreover, the developed K_s model outperforms the Mishra and Parker model. Therefore, the developed method will enable one to substantially reduce the feasible range of the inverted Kosugi's hydraulic parameters.

Key Words: Saturated hydraulic conductivity, Kosugi model, tortuosity, hydraulic parameters, uncertainties, inverse modeling

(*Soil Sci* 2013;178: 267–280)

An attractive cost-efficient alternative to derive the effective soil hydraulic parameters of hydrological models using Richards' equation for layered soil profiles (e.g., Sonnleitner et al., 2003; Mohanty and Zhu, 2007; Wollschläger et al., 2009) is by numerical inversion of space-time series data, for example, volumetric soil water content and/or actual evapotranspiration (e.g., Romano, 1993; Romano and Santini, 1999; Pollacco, 2005; Das and Mohanty, 2006; Das et al., 2008; Ines and Mohanty, 2008a, 2008b, 2008c; Pollacco et al., 2008; Pollacco and Mohanty, 2012; Shin et al., 2012) or from water infiltration experiments (e.g., Lassabatere et al., 2006, 2009, 2010; Cannavo et al., 2010; Yilmaz et al., 2010, 2013; Nasta et al., 2012). Nevertheless, one of the drawbacks of using Richards' equation is that analytical, generally unimodal, expressions are required to describe the soil water retention, $\theta(h)$, and hydraulic conductivity, $K(\theta)$, functions (e.g., Brooks and Corey, 1964; van Genuchten, 1980; Kosugi, 1994). These functions are identified by as many as five fitting hydraulic parameters for each layer of the considered soil profile. Moreover, the feasible range of the effective parameters has to be set within its full feasible range because, in most cases, there is no availability of additional basic soil information that helps to better constrain the parameter space (Scharnagl et al., 2011). Therefore, the inverted hydraulic parameters produce inevitably nonunique solutions (Pollacco et al., 2008; Pollacco and Mohanty, 2012). In addition, the boundary and initial conditions are often not well defined, and the observed data are also affected by relatively large measurement errors (Vrugt et al., 2008). To obtain a unique set of solutions when the hydraulic parameters of soil vegetation atmosphere transfer (SVAT)–type models are inverted from observed root-zone soil moisture data, Pollacco et al. (2008) showed that soil water content, θ, data are required, ranging from very dry to very wet soil conditions. If this condition is not met, then the inversion is prone to yield nonunique hydraulic parameter sets (e.g., Kabat et al., 1997; Abbaspour et al., 1999; Jhorar et al., 2002; Binley and Beven, 2003; Ritter et al., 2003; Minasny and Field, 2005; Beydoun and Lehmann, 2006; Pollacco et al., 2008). Consequently, high uncertainties in the forwarded water fluxes occur (Pollacco and Mohanty, 2012). Thus, it is important to propose new approaches to reduce the nonuniqueness of the inverted hydraulic parameter sets.

A crucial part of the success of an inverse modeling process is to tighten the feasible parametric range such that an adequate minimum and maximum range for each individual parameter is provided. This can be performed by taking into consideration that the value of the saturated hydraulic conductivity, K_s (L T^{-1}), is highly dependent on the values of the other parameters describing the soil water retention $\theta(h)$ function. The proposed method would thus enable to reject all those nonbehavioral parameter sets generated by the optimization algorithm, which do not satisfy soil physically based relations. It is expected that running only those sequences that satisfy this condition would certainly concentrate the optimization search and therefore decrease the uncertainty of the inverted effective parameters.

Several efforts can be found in the literature for estimating K_s from parameters describing $\theta(h)$. For instance, Guarracino (2007) and Mishra and Parker (1990) derived models of K_s for van Genuchten's $\theta(h)$ based on some of the assumptions of Childs and Collis-George (1950) who considered that the soil pore network is made up of a bundle of capillary tubes of different sizes and that the water flow rate can be computed by

[1]Department of Biological and Agricultural Engineering, Texas A&M University, College Station, Texas, USA.
[2]Department of Agriculture, Division of Agricultural, Forest and Biosystems Engineering-University of Napoli Federico II, Naples, Italy.
[3]Departamento de Ingeniería en Geomática e Hidráulica-Universidad de Guanajuato, Guanajuato, Mexico.
[4]Université de Lyon, CNRS, UMR 5023 LEHNA, ENTPE, F-69518, Vaulx-en-Velin, France.
Address for correspondence: Dr. Joseph Alexander Paul Pollacco, PhD, Department of Biological and Agricultural Engineering, Texas A&M University, College Station, TX 77843, USA; E-mail: pollacco.water@gmail.com
The authors report no conflicts of interest.
Received December 7, 2012.
Accepted for publication June 26, 2013.

ISSN: 0038-075X
DOI: 10.1097/SS.0b013e3182a2da21

Hagen-Poiseuille's equation combined with the Darcy law. Guarracino (2007) derived a relation between K_s and van Genuchten's shape parameter, α, assuming that the soil porosity is represented by an equivalent bundle of parallel capillary tubes with a distribution of pore sizes following a fractal law (Tyler and Wheatcraft, 1990; Yu et al., 2003). Mishra and Parker (1990) developed a simple closed-form expression of K_s by using the model by Mualem (1976) coupled to the capillary water retention function of van Genuchten (1980). An additional example of a K_s model is that of Han et al. (2008) based on the inflection point of $\theta(h)$ curve. It is interesting to note that both models proposed by Guarracino (2007) and Mishra and Parker (1990) are similar, although they were developed from different principles.

In this study, we develop a novel model to predict K_s (hereinafter referred as the developed K_{s_dev} model) from knowledge of the four parameters featured in Kosugi's water retention function, namely, θ_s, θ_r, h_m, and σ (Kosugi, 1994, 1996). We selected Kosugi's $\theta(h)$ and $K(\theta)$ lognormal functions partly because Hayashi et al. (2006) found a correlation between the variance (σ) of the log-transformed soil pore radius and the mean log-transformed soil pore radius (R_m) for forest soils, thus enabling to further reduce the feasible parameter space. A peculiarity of Kosugi's model is that its parameters possess physical meanings and have a close link to the soil pore-size distribution. The K_{s_dev} model is based on the approach of Childs and Collis-George (1950), except that the soil water flux goes through a pore network having the hypothetical pore-size distribution of Kosugi (1996). We combined the Hagen-Poiseuille equation with Darcy law and incorporated three tortuosity parameters. The first two parameters are those of Fatt and Dykstra (1951), whereas the third one is derived according to Vervoort and Cattle (2003) to account for higher porosity media that tend to be more connected than lower porosity media. We compare K_{s_dev} with the Mishra and Parker (1990) (K_{s_mish}) model but adapted it so as it can account for the Kosugi model.

Moreover, we later present a simplified K_{s_dev} ($K_{s\_dev\_\sigma}$) by exploiting the correlation between σ and R_m (Hayashi et al., 2006). Thus, $K_{s\_dev\_\sigma}$ will be computed from three parameters only, which are θ_s, θ_r, and h_m. The predicted values are compared with experimental data from the UNSODA (e.g., Leij et al., 1999; Schaap and van Genuchten, 2006) and the HYPRES (e.g., Wösten et al., 1998, 1999; Lilly et al., 2008) large databases. We selected soil samples that contain data on $\theta(h)$, $K(\theta)$, K_s, and θ_s (or porosity).

In summary, the article is organized as follows:

1) To develop a new saturated hydraulic conductivity model based on the Kosugi (1996) model (K_{s_dev});
2) To use the Kosugi (1996) analytical relationship in the Mishra and Parker (1990) K_s model (K_{s_mish});
3) To propose a K_s model that makes use of only three parameters of the Kosugi analytical relations ($K_{s\_dev\_\sigma}$);
4) To select data sets from UNSODA and HYPRES according to set criteria;
5) To optimize the Kosugi hydraulic parameters simultaneously from available $\theta(h)$ and $K(\theta)$ data sets;
6) To determine the uncertainty bands of the model predictions.

THEORY

Kosugi Model

Kosugi (1996) developed a physically based lognormal function $p(R) = d\theta/dR$ (L^{-1}) for describing the distribution of pore sizes (R). Specifically, the lognormal probability density function of pore radius can be written as follows:

$$\frac{d\theta}{dR} = \frac{\theta_s - \theta_r}{R\sigma\sqrt{2\pi}} \exp\left\{-\frac{(\ln R - \ln R_m)}{2\sigma^2}\right\} \quad (1)$$

where θ_r and θ_s ($L^3\ L^{-3}$) are the residual and saturated water contents, respectively, such that $\theta_r \le \theta \le \theta_s$; $\ln(R_m)$ and σ^2 are the mean and variance of the log-transformed soil pore radius, $\ln(R)$, respectively.

Let S_e denote the effective saturation, such that $0 \le S_e \le 1$. Therefore $p(R)\cdot dR$ represents the contribution of the filled pores of radius $R \rightarrow (R + dR)$ to the effective saturation. Integrating Eq.(1) from 0 to R yields the water retention curve, which is a function of R:

$$S_e(R) = \frac{1}{2} erfc\left[\frac{\ln R_m - \ln R}{\sigma\sqrt{2}}\right] \quad (2a)$$

or

$$R = \frac{R_m}{\exp\left[erfc^{-1}(2S_e)\sigma\sqrt{2}\right]} \quad (2b)$$

where

$$S_e = \frac{\theta-\theta_r}{\theta_s-\theta_r} \quad (3)$$

In Eq.(2), *erfc* denotes the complementary error function.

The well-known Young-Laplace capillary equation enables the soil pores radius, R, to be uniquely related to the equivalent matric suction head, h (cm), at which the pore is filled or drained (i.e., $R = Y/h$, with $Y = 0.149\ cm^2$). The Kosugi water retention function has the following analytical expression for S_e:

$$S_e = \frac{1}{2} erfc\left[\frac{\ln h - \ln h_m}{\sigma\sqrt{2}}\right] \quad (4a)$$

or

$$h = h_m \exp\left[erfc^{-1}(2S_e)\sigma\sqrt{2}\right] \quad (4b)$$

where $\ln(h_m)$ and σ denote the mean and S.D. of $\ln(h)$, respectively.

The relative hydraulic conductivity, K_r (0, 1), can be written in terms of pore-size distribution of soil, as follows (Mualem (1976):

$$K_r(h) = S_e^{0.5}\left[\frac{\int_0^{S_e}\frac{Y}{h}\,dS_e}{\int_0^1\frac{Y}{h}\,dS_e}\right]^2 \quad (5)$$

where Y is the Young-Laplace constant described above.

The unsaturated hydraulic conductivity function can be obtained (Kosugi et al., 2002) by introducing h of Eq.(4) into Eq.(5):

$$K(S_e) = K_s K_r(S_e) = K_s S_e^{0.5}\left\{\frac{1}{2} erfc\left[erfc^{-1}(2S_e) + \frac{\sigma}{\sqrt{2}}\right]\right\}^2 \quad (6)$$

Development of a Saturated Hydraulic Conductivity Model: K_{s_dev}

Under full saturation condition, K_s can be obtained from the Darcy (1856) law as follows:

$$K_s = q\frac{L}{\Delta H} \tag{7}$$

where q ($L\,T^{-1}$) is the average water flux, ΔH is the total hydraulic head (L), L (L) is the path length in the direction of the flow.

An alternative model to quantify the flow rate into the soil is based on the representation of the porous medium as a bundle of parallel nonintersecting capillary tubes. The volumetric flow rate, Q_i ($L^3\,T^{-1}$), in each capillary tube of radius R_i is calculated through Hagen-Poiseuille equation (Bear, 1972):

$$Q_i = C\ \pi\ \frac{\Delta H}{L_{\tau_i}}\ R_i^4 \tag{8}$$

with

$$C = \frac{1}{8}\ \frac{\rho_w g}{\eta}$$

where, for water at 20°C, ρ_w = 0.998 g cm^{-3} density of water, g = 980.66 cm s^{-2} is the acceleration caused by gravity; η = 0.0102 g cm^{-1} sec^{-1} is the dynamic viscosity of water, where C is a constant equal to 1.03663×10^9 cm d^{-1}; $\Delta H/L_{\tau_i}$ ($L\,L^{-1}$) represents the gradient of the total hydraulic head between the two ends of the capillary tube; and L_{τ_i} (cm) is the effective twisted path length of the ith capillary tube over which the fluid travels so $L_{\tau_i} > L$.

The total flux density through the column, when all the tubes are filled, is the sum of the flux densities passing through each pore size class. Let N_i be the number of capillary tubes having a radius R_i. Therefore, the specific flux of water, q ($L\,T^{-1}$) is defined as the volumetric discharge per unit cross-sectional area (A) and can be expressed as:

$$\begin{aligned} q &= \frac{Q}{A} = C\ \sum_{i=1}^{I}\frac{\Delta H}{L_{\tau_i}}\ \frac{N_i}{A}\ \pi\ R_i^4 \\ &= C\ \sum_{i=1}^{I}\frac{\Delta H}{L_{\tau_i}}\ n_i\ \pi\ R_i^4 \end{aligned} \tag{9}$$

where I is the total number of class R_i in the bundle and where $n_i = N_i/A$ is the number of capillary tubes per unit area in each class.

K_s is computed by introducing q given by Eq.(9) into Eq.(7):

$$K_s = C\ \sum_{i=1}^{I}\frac{L}{L_{\tau_i}}\ n_i\ \pi\ R_i^4 \tag{10}$$

The change of soil moisture $\Delta\theta_i$ ($L^3\ L^{-3}$) when n_i capillary tubes of cross-sectional area $\pi\ R_i^2$ drain is computed for each pore size class i by:

$$\Delta\theta_i = \Delta S_{e,i}\ (\theta_s - \theta_r) \tag{11}$$

or

$$\Delta\theta_i = n_i\ \pi\ R_i^2$$

We introduced a tortuosity model into the K_s model. Fatt and Dykstra (1951) proposed the following equation written with our terminology:

$$L_{\tau_i} = L\ \tau_1'\ R_i^{\ \tau_2'} \tag{12}$$

or

$$\frac{L}{L_{\tau_i}} = \frac{R_i^{\ -\tau_2'}}{\tau_1'}$$

where τ_1', τ_2' [-] are optimized tortuosity parameters that were taken from Eq.(11) and Eq.(12) of Fatt and Dykstra (1951) for which the constant a is substituted for τ_1' and the exponent b is substituted for τ_2'.

Isolating n_i of Eq.(11), and substituting it into Eq.(10) and introducing $L/\ L_{\tau_i}$ (Eq.(12)) into Eq.(10) gives:

$$K_s = \frac{1}{\tau_1'}\ C\ (\theta_s - \theta_r)\ \sum_{i}^{I} R_i^{2-\tau_2'}\ \Delta S_{e,i} \tag{13}$$

or

$$K_s = \ \tau_1\ C\ (\theta_s - \theta_r)\ \sum_{i}^{I} R_i^{\tau_2}\ \Delta S_{e,i}$$

where τ_2 is a tortuosity parameter that adjusts the shape of the capillary tube such that $\tau_2 = 2 - \tau_2'$ with $0 < \tau_2 < 2$. When $\tau_2' = 0$, the capillary tube is perfectly cylindrical, whereas when $2 > \tau_2' > 0$, the tube changes into the "actual" shape. The tortuosity of the tubes with the radius R_i defined by L/L_{τ_i} should be smaller than 1. Therefore, because $R < 1$, then $\tau_1' > 1$ and $\tau_1 \leq 1$ since $\tau_1 = (\tau_1')^{-1}$.

Vervoort and Cattle (2003) state that in high-porosity media, the large effective pores tend to be more connected than the smaller effectives pores. Thus, smaller effective pores should have a smaller connectivity than larger effective pores. Therefore, we introduce another tortuosity parameter τ_3 to the power of (θ_s - θ_r) as in many empirical K_s models (e.g., Messing, 1989; Mishra and Parker, 1990; Han et al., 2008). The K_s model is then written as:

$$K_s = \tau_1\ C\ (\theta_s - \theta_r)^{\tau_3}\ \sum_{i}^{I} R^{\tau_2}\ \Delta S_{e,i} \tag{14}$$

where τ_3 is a fitting parameter, such that $(\theta_s - \theta_r) > (\theta_s - \theta_r)^{\tau 3}$ hence $\tau_3 \geq 1$, to take into account a reduction of K_s caused by reduced connectivity of smaller pores.

Isolating R of Eq.(2b) and substituting it into Eq.(14) and writing the equation into a continuous derivative form give the developed K_{s_dev} model:

$$K_{s\_dev} = \tau_1\ C\ (\theta_s - \theta_r)^{\tau_3}\ R_m^{\ \tau_2}\ \int_0^1 \left\{\frac{1}{\exp\ \left[erfc^{-1}(2\ S_e)\ \sigma\sqrt{2}\right]}\right\}^{\tau_2} dS_e \tag{15a}$$

Or likewise isolating h of Eq.(2b) and substituting it into Eq. (14) by using the Young-Laplace capillary equation to relate R with h and writing the equation into a continuous derivative form gives the developed K_{s_dev} model:

$$K_{s\_dev} = \tau_1\ C\ (\theta_s - \theta_r)^{\tau_3}\ \left(\frac{Y}{h_m}\right)^{\tau_2} \int_0^1 \left\{\frac{1}{\exp\ \left[erfc^{-1}(2\ S_e)\ \sigma\sqrt{2}\right]}\right\}^{\tau_2} dS_e \tag{15b}$$

In summary, the three tortuosity parameters of the K_s model in Eq.(15): $\tau 1 \in (0, 1)$, $\tau 2 \in (0, 2)$, and $\tau_3 \in (1, 10)$, will be optimized for different soil types found in two large databases described below.

Modified Mishra and Parker Saturated Hydraulic Conductivity Model: K_{s_mish}

Mishra and Parker (1990) proposed a K_s model that is computed from knowledge of the van Genuchten (1980) soil hydraulic parameters. We have adjusted the Mishra and Parker (1990) K_s model so as it can account for the Kosugi (1996) soil hydraulic parameters. An integral formulation of the unsaturated hydraulic conductivity of Mualem (1976) and Mualem and Dagan (1978) can be described following Mishra and Parker (1990) as:

$$K(S_e) = \tau_1 \; C \; (\theta_s - \theta_r)^{5/2} \; \sqrt{S_e} \; \left[\int_0^{S_e} \frac{1}{h} \; dS_e\right]^2 \quad (16)$$

where τ_1 is a tortuosity parameter for which Corey (1979) gives a value of 2/5. Nevertheless, in this study, τ_1 is taken as a fitting parameter.

Isolating h of the characteristic curve (Eq.(4b)), introducing it into Eq.(16), and considering the specific case of saturated conditions ($S_e = 1$) give the modified Mishra and Parker K_{s_mish} model:

$$K_{s\_mish} = \tau_1 C (\theta_s - \theta_r)^{5/2}$$

$$R_m{}^2 \left(\int_0^1 \frac{1}{\exp\left[erfc^{-1}(2 \; S_e) \; \sigma\sqrt{2}\right]} \; dS_e \right)^2 \quad (17a)$$

or

$$K_{s\_mish} = \tau_1 C (\theta_s - \theta_r)^{5/2}$$

$$\left(\frac{Y}{h_m}\right)^2 \left(\int_0^1 \frac{1}{\exp\left[erfc^{-1}(2 \; S_e) \; \sigma\sqrt{2}\right]} \; dS_e \right)^2 \quad (17b)$$

We highlight (as shown in Table 1) that K_{s_mish} is similar to K_{s_dev}. The major difference is because the exponent τ_2 of K_{s_dev} is inside the integral, whereas the "τ_2" = 2 of K_{s_mish} is outside the integral. The K_{s_dev} has three fitting parameters, whereas K_{s_mish} has only one. The feasible range of the parameters of the two models is summarized in Table 2.

TABLE 2. Feasible Range of the Parameters of the K_s Models and the Predictive σ_p Model

Model	Equation	Parameters	Minimum	Maximum
K_s	Eq.(15) and Eq.(17)	τ_1	0.1	1.0
	Eq.(15)	τ_2	0.1	1.9
		τ_3	1.0	10.0
σ_p	Eq.(18)	$P_{\sigma 1}$	0.1	1.0
		$P_{\sigma 2}$	0.1	1.0

Reducing the Feasible Parameter Space of σ

To reduce the feasible parameter space of σ, we exploit the finding of Hayashi et al. (2006) who found a correlation between R_m and σ for forest soils (high porosity). Nevertheless, Hayashi et al. (2006) did not verify their relationship for other soils. To verify this relationship for contrasting soils, we plotted in Fig. 1 the relationship between $\log_{10} R_m$ and σ. The R_m and σ Kosugi parameters values are obtained from 73 soil data sets, which will be described later. Figure 1 clearly shows that there is a negative linear correlation between $\log_{10} R_m$ and σ with $R^2 = 0.63$. Thus, the tendency is that the larger median pore size (R_m), which is representative of coarse structure soils, is related to the smaller standard distribution (dispersion) of the pore size σ. This behavior can be explained by the fact that when R_m is large, the soil tends to be composed of a single-grained structure (monodisperse) and thus σ tends to be small. Conversely, when R_m is reduced, which is representative of finer material (characterized by a more tortuous structure (Fatt and Dykstra, 1951; also refer to Eq.(12)), then the soil structure is aggregated and the soil is mostly composed of an array of grain sizes (polydisperse) and, therefore, σ has a larger dispersion. To reduce the

TABLE 1. Summary of Models Tested in This Work

Model	Equation	Parameter
$K_{s\_dev} = \tau_1 \; C \; (\theta_s - \theta_r)^{\tau_3} \; R_m{}^{\tau_2} \int_0^1 \left\{ \frac{1}{\exp\left[erfc^{-1}(2 \; S_e) \; \sigma\sqrt{2}\right]} \right\}^{\tau_2} dS_e$	Eq.(15)	3
$K_{s\_mish} = \tau_1 \; C \; (\theta_s - \theta_r)^{5/2} \; R_m{}^2 \left(\int_0^1 \frac{1}{\exp\left[erfc^{-1}(2 \; S_e) \; \sigma\sqrt{2}\right]} \; dS_e \right)^2$	Eq.(17)	1
$\sigma_p = P_{\sigma 1} \left[\mathrm{Ln} \left(\frac{Y}{R_m}\right) - 1\right]^{P_{\sigma 2}}$	Eq.(18)	2
$K_{s\_dev\sigma} = \tau_1 \; C \; (\theta_s - \theta_r)^{\tau_3} \; R_m{}^{\tau_2} \int_0^1 \left\{ \frac{1}{\exp\left[erfc^{-1}(2S_e) \quad P_{\sigma 1} \left[\mathrm{Ln} \left(\frac{Y}{R_m}\right) - 1\right]^{P_{\sigma 2}} \sqrt{2}\right]} \right\}^{\tau_2} dS_e$	Eq.(19)	5

The feasible ranges of the related parameters are presented in Table 2.

K_{s_dev}: the developed K_s model; K_{s_mish}: the modified Mishra and Parker K_s model; σ_p: the predictive σ model; $K_{s\_dev\_\sigma}$: the implementation of the σ_p into K_{s_dev}.

feasible parameter space of Kosugi parameters, we hereby propose the following equation based on Fig. 1, which links predicted σ (σ_p) with R_m:

$$\sigma_p = P_{\sigma 1}\left[\ln\left(\frac{Y}{R_m}\right)-1\right]^{P_{\sigma 2}} \quad (18a)$$

or

$$\sigma_p = P_{\sigma 1}\left(\ln h_m - 1\right)^{P_{\sigma 2}} \quad (18b)$$

where $P_{\sigma 1}$ and $P_{\sigma 2}$ are two fitting parameters. Because $0 < \sigma < 5$ and $\ln h_m > 2.5$, then $P_{\sigma 1}$ and $P_{\sigma 2}$ should be between 0 and 1. The summary of the feasible range of the parameters is described in Table 2.

Reducing the Feasible Parameter Space of K_{s_dev}: $K_{s\_dev\_\sigma}$

The $K_{s\_dev\_\sigma}$ exploits the relationship of Eq.(18) to reduce the number of input Kosugi parameters from four (θ_r, θ_s, σ, R_m *or* h_m) to three (θ_r, θ_s, R_m *or* h_m). The $K_{s\_dev\_\sigma}$ is computed by inputting $\sigma_p(h_m)$ (Eq.(18)) into Eq.(15):

$$K_{s\_dev\_\sigma} = \tau_1\ C\ (\theta_s-\theta_r)^{\tau_3}\ R_m^{\tau_2} \int_0^1 \left\{\frac{1}{\exp\left[erfc^{-1}(2S_e)\,P_{\sigma 1}\left[\ln\left(\frac{Y}{R_m}\right)-1\right]P_{\sigma 2}\sqrt{2}\right]}\right\}^{\tau_2} dS_e \quad (19a)$$

or

$$K_{s\_dev\_\sigma} = \tau_1\ C\ (\theta_s-\theta_r)^{\tau_3}\left(\frac{Y}{h_m}\right)^{\tau_2} \int_0^1 \left\{\frac{1}{\exp\left[erfc^{-1}(2\ S_e)\,P_{\sigma 1}\left[\ln(h_m)-1\right]^{P_{\sigma 2}}\sqrt{2}\right]}\right\}^{\tau_2} dS_e \quad (19b)$$

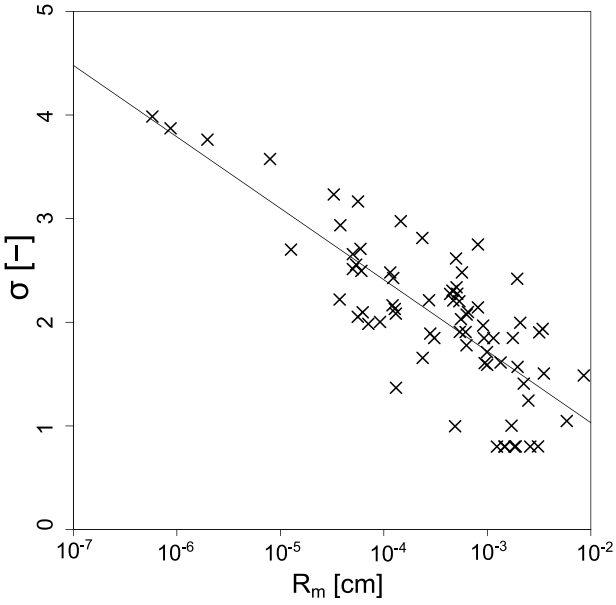

FIG. 1. Linear relationship between the S.D. of log-transformed matric potential head (σ) and the parameter of pore-radius distribution R_m ($\log_{10}$ scale).

The optimal parameters τ_1, τ_2, τ_3 are retrieved from K_{s_dev} model (Eq.(15)), and the parameters $P_{\sigma 1}$, $P_{\sigma 2}$ are taken from σ_p (Eq.(18)). A summary of the different models is shown in Table 1.

MATERIALS AND METHODS

Step 1: Criteria for Selecting Soils From the UNSODA and HYPRES Databases

We selected 318 soil data from the UNSODA database (Leij et al., 1999; Schaap and van Genuchten, 2006) and the HYPRES (Wösten et al., 1998, 1999; Lilly et al., 2008), providing $\theta(h)$ and $K(\theta)$ measured data points, including measured values for K_s and θ_s. In the case where θ_s was not available, this parameter was calculated from knowledge of porosity, ϕ, as follows:

$$\theta_s = 0.95\ \varphi \quad (20)$$

where 0.95 was obtained through a linear regression analysis (results not shown).

From the 318 soils, we selected 73 data sets that comply with the selection criteria described in Table 3. The number of soils selected after we performed the different filtering clearly shows that criterion A is the most important to ensure the required standards of the data sets. The 73 selected data sets were corrected so that if $\theta_i(h) > \theta_s$, then $\theta_s = \theta_i(h)$, and likewise if $K_i(\theta) > K_s$, then $K_s = K_i(\theta)$.

Step 2: Inverse Modeling

A robust global optimization algorithm AMALGAM written in MATLAB (http://faculty.sites.uci.edu/jasper/sample/) (e.g., ter Braak and Vrugt, 2008; Vrugt and ter Braak, 2011) was used to: (i) inversely estimate the Kosugi parameters from the observed $\theta(h)$ and $K(\theta)$ data points; (ii) optimize the parameters of the saturated hydraulic conductivity models (K_{s_dev}, $K_{s\_dev\_\sigma}$, K_{s_Mish}; Table 1); (iii) optimize the parameters of the regression sigma model (σ_p). For each of these models, we required to maximize the objective functions described below, which corresponds to minimize the distance between predicted and observed values.

Inverting the Soil Hydraulic Parameters From the Characteristic and Unsaturated Hydraulic Conductivity Curves

The θ_r, h_m, and σ parameters are optimized by maximizing a weighted objective function (WOF), which is described below. The feasible parameter space of these parameter sets is described in Table 4. The WOF is composed of two objective functions (OF): the first term, OF_θ, is computed with observed and predicted $\theta(h)$ values, and the second term, OF_k, is calculated with observed and predicted $K(\theta)$ values. To account for the differences in magnitude between the two criteria, they are normalized according to the Nash-Sutcliffe (1970) efficiency (NSE) formulation such that the optimal minimum is reached when the WOF is equal to 1. The Nash and Sutcliffe (1970) WOF is described as:

$$WOF = \frac{1}{2}\ OF_{\theta}\ + \frac{1}{2}\ OF_{k} \tag{21a}$$

with:

$$OF_{\theta} = \sqrt{1 - \frac{\sum_{i=1}^{i=N_{\theta}} \left[\theta_p(h_i, \mathbf{P}_{\theta}) - \theta_{obs}(h_i)\right]^2}{\sum_{i=1}^{i=N_{\theta}} \left[\theta_{obs}(h_i) - \overline{\theta_{obs}(h_i)}\ \right]^2}}$$

$$OF_{k} = \sqrt{1 - \frac{\sum_{j=1}^{j=N_{k}} \left[\ln\ K_p(Se_i, \mathbf{P}_{\mathbf{k}}) - \ln\ K_{obs}(Se_i)\right]^2}{\sum_{j=1}^{j=N_{k}} \left[\ln\ K_{obs}(Se_i) - \ln\ \overline{K_{obs}(Se_i)}\right]^2}} \tag{21b}$$

where the subscripts p and obs are predicted and observed, respectively. The $\mathbf{P}_{\boldsymbol{\theta}}$ and $\mathbf{P}_{\boldsymbol{k}}$ are the set of predicted parameters (h_m, σ, R_m, θ_r) of $\theta(h)$ and $K(\theta)$, respectively. One is reminded that θ_s and K_s are directly obtained from the data; values for N_{θ} and N_K correspond to the total number of data pairs for (h_i, θ_i) and (Se_i, K_i), respectively. The θ_p and K_p are described through Eq.(4) and Eq.(6), respectively. The log transformation of OF_k puts relatively more weight on the lower $K(\theta)$ and therefore minimizes the bias toward high conductivity (e.g., Van Genuchten et al., 1991). Also the log transformation takes into account that the uncertainties in measuring the unsaturated hydraulic conductivity increases as $K(\theta)$ increases. It is to be noted that the global optimizer obtains better results when the natural logarithm transformation (ln) is used instead of the decimal logarithm transformation ($\log_{10}$) of $K(\theta)$. This is because, for the computation of OF_k, the natural log is more sensitive than the $\log_{10}$.

The usage of Nash and Sutcliffe (1970) objective function enables us to reject nonbehavioral soils, that is, soils that do not comply with the $\theta(h)$ and $K(\theta)$ Kosugi model. Thus, soils were also rejected on the premise that $OF_{\theta} < 0.1$ or $OF_K < 0.1$ so that only 73 suitable soil data sets were retained to parameterize the K_s models (Table 3).

Inverting the Parameters of the Saturated Hydraulic Conductivity Models

The "physical" feasible range of the fitting parameters of the K_{s_dev} (Eq.(15)) and K_{s_mish} (Eq.(17)) models are provided in Table 2. The parameters are optimized by maximizing the objective function OF_{ks} of Nash and Sutcliffe (1970):

$$OF_{ks\_dev} = \sqrt{1 - \frac{\sum_{j=1}^{j=N_{ks}} \left[\ln\ K_{s\_dev}(\mathbf{P_{ks}}) - \ln\ K_{s\_obs}\right]^2}{\sum_{j=1}^{j=N_{ks}} \left[\ln\ K_{s\_obs} - \overline{\ln\ K_{s\_obs}}\ \right]^2}} \tag{22a}$$

$$OF_{ks\_mish} = \sqrt{1 - \frac{\sum_{j=1}^{j=N_{ks}} \left[\ln\ K_{s\_mish}(\mathbf{P_{ks}}) - \ln K_{s\_obs}\right]^2}{\sum_{j=1}^{j=N_{ks}} \left[\ln\ K_{s\_obs} - \overline{\ln\ K_{s\_obs}}\ \right]^2}} \tag{22b}$$

where $\mathbf{P_{ks}}$ is the vector of the unknown parameters of the K_{s_dev} (i.e., (τ_1, τ_2 , τ_3), and τ_1 for K_{s_mish}; K_{s_obs} is observed saturated hydraulic; N_{ks} is the number of K_s measured data).

Inverting the Parameters of the (R_m and σ) Regression Model

The feasible range of the fitting parameters of the σ model described in Eq.(18) is provided in Table 2. The optimization of the parameters for the σ model is performed by maximizing the Nash and Sutcliffe (1970) objective function, which is computed as:

$$OF_{\sigma} = \sqrt{1 - \frac{\sum_{i=1}^{i=N_{\sigma}} \left[\sigma_p(\mathbf{p}_{\sigma}) - \sigma\right]^2}{\sum_{i=1}^{i=N\sigma} \left[\sigma - \overline{\sigma}\right]^2}} \tag{23}$$

where $\mathbf{P_{\sigma}}$ is the vector of unknown parameters ($P_{\sigma 1}$ and $P_{\sigma 2}$) of the regression sigma model; σ_p and σ (cm) are predicted and fitted σ (by maximizing WOF) parameters respectively; N_{σ} is the number of samples.

Uncertainties in Saturated Hydraulic Conductivity Measurements

Estimating the uncertainties embedded in the measurement of K_s is challenging because K_s is highly variable (e.g., Mohanty et al., 1994a; Upchurch et al., 1988 ; Suwardji and Eberbach, 1998; Bormann and Klaassen, 2008) and is also scale dependent (e.g., Mallants et al., 1997; Sobieraj et al., 2004; Das Gupta et al., 2006). In addition, the K_s value is specially dependent on the measurement method used, as shown by Mohanty et al. (1994b) and Fodor et al. (2011) who evaluated the

TABLE 3. Criteria for the Selection of Soils From the UNSODA and HYPRES Databases

	Description	*n*
A	In soils, the effective water-filled pore sizes decrease with desaturation. Therefore, the measured $\theta(h)$ and $K(\theta)$ can only strictly decrease as the capillary suction increases (Peters et al., 2011). Exception is given for the first two points near saturation.	138
B	Soils with at least 6 $\theta(h)$ and 6 $K(\theta)$ data points.	271
C	Soils that have at least one data point near saturation such that $S_e \geq 0.7$ and $K_r(h) \geq 0.7$	301
D	Soils in which $0.3 < \theta_s < 0.8$ m^3 m^{-3}	304
E	**A ∩ B ∩ C ∩ D**	88
F	Soils matching E and with $OF_{\theta} > 0.1$ and $OF_K > 0.1$ after inverse modeling	73

Where OF_{θ} and OF_K are the Nash and Sutcliffe (1970) objective functions for $\theta(h)$, $K(\theta)$, respectively, and described in Eq.(21), where *n* is the number of soils.

TABLE 4. Typical Feasible Range of the Optimized Parameters of the Kosugi Model Described in Eq.(4) and Eq.(6) That Was Used for Optimization

	θ_r, $m^3\ m^{-3}$	$\log_{10} h_m$, cm	$\log_{10} R_m$, cm	σ, cm
Minimum	0	1.1	−6.5	0.7
Maximum	0.25	6	−2	5

Where h_m and R_m are linked through the Young-Laplace capillary equation.

measurement errors by applying different methods (double ring, Guelph, velocity, tension disc, and mini disc infiltrometers and other laboratory methods). Fodor et al. (2011) found that the errors in measuring K_s are estimated to be $\pm 1 \times 10^{1.3}$ cm d^{-1}. On the other hand, Minasny and Field (2005) assessed the errors of deriving K_s from laboratory experiments (like the evaporation method) combined with the generalized likelihood uncertainty estimation (GLUE) inverse procedure for estimating *K(θ)* and *θ(h)*, and they found that the uncertainties are approximately $\pm 1 \times 10^{1.0}$ cm d^{-1}. Moreover, to take the uncertainties associated to the scale effect into account, as well as the spatial and temporal variability of K_s, we assumed that the errors in obtaining K_s could be of the order of $\pm 1 \times 10^{1.8}$ cm d^{-1}, a value to which we will refer to evaluate the goodness of our developed K_s model.

It is interesting to note that, although there are large uncertainties in measuring K_s because it is retrieved indirectly through the Darcy law, that K_s is also the least sensitive soil parameter when inverted (e.g., Ines and Droogers, 2002; Beydoun and Lehmann, 2006; Pollacco et al., 2008; Pollacco and Mohanty, 2012). Furthermore, Pollacco et al. (2008) showed that if K_s contains uncertainty, then the other parameters of the *θ(h)* would be adjusted during the optimization to correct for the modeled K_s without greatly influencing the computation of the water fluxes (Pollacco and Mohanty, 2012).

RESULTS

Optimized Hydraulic Parameters

The UNSODA and HYPRES soil databases were filtered with the rules described in Table 3 and from the resulting 73 data sets; the Kosugi hydraulic parameters (θ_r, h_m, and σ) were optimized by maximizing WOF (Eq.(21)). The descriptive statistics of the optimized hydraulic parameters as well as of the measured θ_s and K_s parameters (obtained directly from the databases) are summarized in Table 5. Although only 73 soils remained after the previously mentioned filtering phase, we observed that the ranges of the hydraulic parameters of the 73 soils are representative of all soil textures and therefore very effective for our evaluations.

The statistical information of the optimization process described in Table 6 shows an overall good agreement between observed and fitted *θ(h)* and *K(θ)* points. As expected, the fitting of *θ(h)* represented by OF_θ (Eq.(21)) is better than the fitting of the log-transformed *K(θ)* described by OF_k (Eq.(21)). These fits allow the optimization of σ. The values of K_{s_obs} were directly derived from the measured values available in the database. The values of σ and K_{s_obs} are then considered as observed experimental data to be modeled with the proposed models described in Table 1. Moreover, statistical analyses show that the probability distribution of K_{s_obs} values follows a lognormal distribution (data not shown).

Results of the Sigma Model

In this section, we model the relationship $\sigma_p(R_m)$ (Eq.(18)) between the average pore radius, R_m, and the pore radius S.D. σ by maximizing OF_σ (Eq.(23)) with respect to the two parameters $P_{\sigma 1}$ and $P_{\sigma 2}$. The fit between observed σ and predicted σ_p is portrayed in Fig. 2A, and the descriptive statistics of the performance of σ_p are described in Table 7. Figure 2A and Table 7 show that σ_p has an acceptable performance, with root mean square errors (RMSE) = 0.45 and NSE = 0.44. In addition, the model can be considered valid because there is no evident correlation between the model errors, E_r, and the predicted values (Fig. 2B).

To compute the 95% confidence interval of σ_p (CL_{95}), we need to determine the type of distributions the residuals of the model, E_r, obey. This is performed by plotting the probability plots of E_r described by the histograms in Fig. 2C, which suggest a normal distribution. This is further confirmed by the Kolmogorov-Smirnov tests ((KST) in Table 7), which attest that the hypothesis of normality cannot be rejected (critical probability KST > 5%). In addition, the residual E_r exhibits mean values close to zero (mean in Table 7). Thus, the residuals of σ_p are normally distributed, and CL_{95} interval can be safely computed as approximately twice the S.D. of E_r (Table 7), which is used to define the uncertainty bands of the proposed sigma model (Fig. 2A). When performing inverse modeling, the feasible range of σ_p, summarized in Table 10, depends on the value of h_m and on the CL_{95}. Thus, $\sigma = \sigma_p(h_m) \pm 0.89$.

Results of the Saturated Hydraulic Conductivity Models

The observed K_{s_obs} is plotted against K_{s_mish}, K_{s_dev}, $K_{s\_dev\_\sigma}$ in Fig. 3A, B, C, respectively. The optimal tortuosity parameters τ_1, τ_2, τ_3 of K_{s_dev} and τ_1 of the K_{s_mish} models are optimized by maximizing OF_{ks} (Eq.(22)). The optimal τ_1, τ_2, τ_3 values, descriptive statistics of the models, and their

TABLE 5. Descriptive Statistics of the Selected (Table 3) Optimized θ_r, h_m, and σ Kosugi Parameters

	θ_s, $m^3\ m^{-3}$	θ_r, $m^3\ m^{-3}$	$\log_{10} h_m$, cm	$\log_{10} R_m$, cm	σ, cm	$\log_{10} K_s$, cm d^{-1}
Minimum	0.32	0.00	1.24	−6.24	0.80	0.19
Maximum	0.71	0.25	5.41	−2.07	3.99	4.62
Mean	0.47	0.11	2.66	−3.49	2.06	3.22
S.D.	0.09	0.08	0.84	0.84	0.73	0.78

The θ_s and K_s values were directly obtained from the data set. The parameters h_m and R_m are linked through the Young-Laplace capillary equation. The maximum value of θ_r was obtained from Table 4. This table shows that the selected soils cover practically the full soil spectrum.

TABLE 6. Statistical Information on the Selected (Table 3) Observed and Fitted $\theta(h)$ and $K(\theta)$ by Using the Objective Function Described in Eq.(21)

	I $\Delta\theta(h)$I	I ΔLog$_{10}$ $K(\theta)$I
NSE	0.92	0.70
RMSE	0.023	0.61
Bias	0.018	0.47
SD_BIAS	0.008	0.60

Where NSE is the Nash-Sutcliffe (1970) efficiency, RMSE is the root mean square error, and STD_BIAS is the S.D. of the bias. The results suggest that there is an excellent fit between observed and simulated $\theta(h)$ and $K(\theta)$.

TABLE 7. Optimal Parameters of σ_p (Eq.(18))

	σ_{mod}
$P_{\sigma 1}$	0.5920
$P_{\sigma 2}$	0.7679
NSE	0.44
RMSE	0.446
R^2	0.624
Bias	0.36
Mean	$-3\ 10^{-3}$
σ_e	0.449
95% CI	±0.89
KST	0.89
Outliers	4

Where NSE is the Nash-Sutcliffe (1970) efficiency coefficient; RMSE is the root mean square error; R^2 is the coefficient of determination; Bias is the bias; Outliers are the number of data points that differ significantly from model predictions. The following statistics are based on the modeled residuals (E_r) computed as the differences between predicted data and observations: KST is the critical probability for Kolmogorov-Smirnov tests test of normality; σ_e is the S.D.; 95% CI is the 95% confidence interval by assuming the errors are lognormal distributed.

performance are provided in Table 8, which clearly shows the ranking of the models based on the NSE coefficient, the correlation coefficient (R^2), RMSE, and bias. All these performance measures show the same conclusions and enable us to rank these models as follows: K_{s_dev} (NSE = 0.71) > $K_{s\_dev\_\sigma}$ (NSE = 0.53) > K_{s_mish} (NSE = 0.39), and therefore, K_{s_dev} outperforms K_{s_mish}. This is mainly because K_{s_dev} has two extra degrees of freedom compared with K_{s_mish}. It would have been expected that the implementation of σ_p model (Eq.(18))

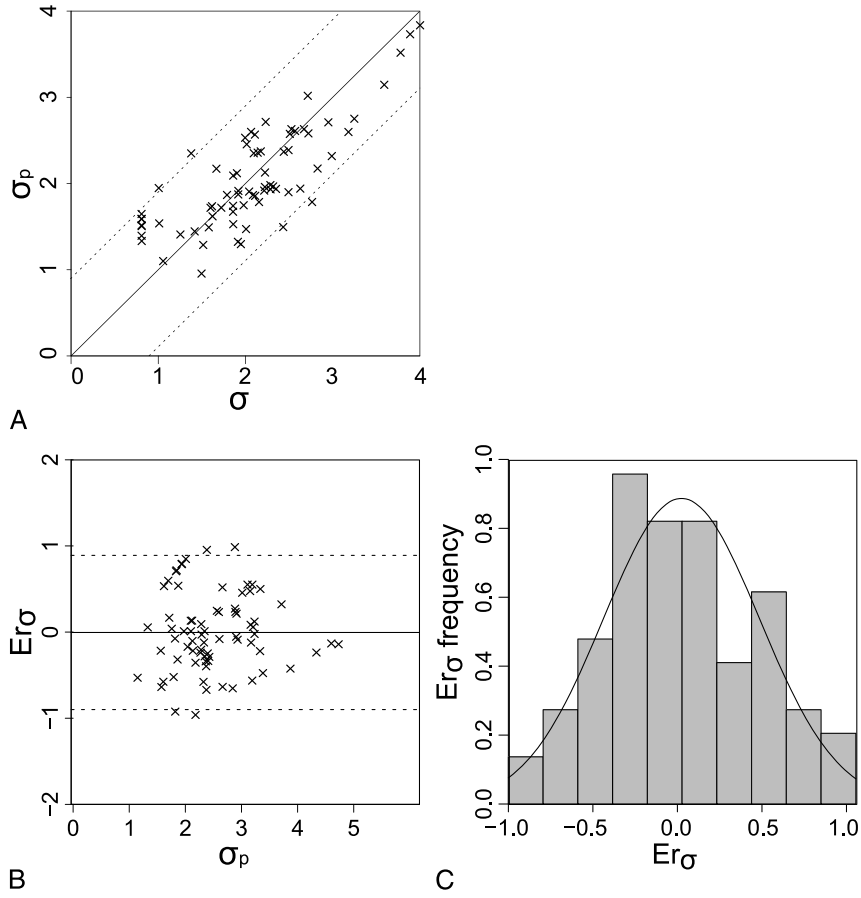

FIG. 2. A, Predicted variance of the log-transformed soil pore radius σ_p (Eq.(18)) with the optimized σ (Eq.(23)), where the dotted lines represent the 95% CI. B, Predicted values, σ_p, as a function of residuals ($E_{r\sigma}$). C, Statistic distribution of residuals (bars) and normal distribution (line).

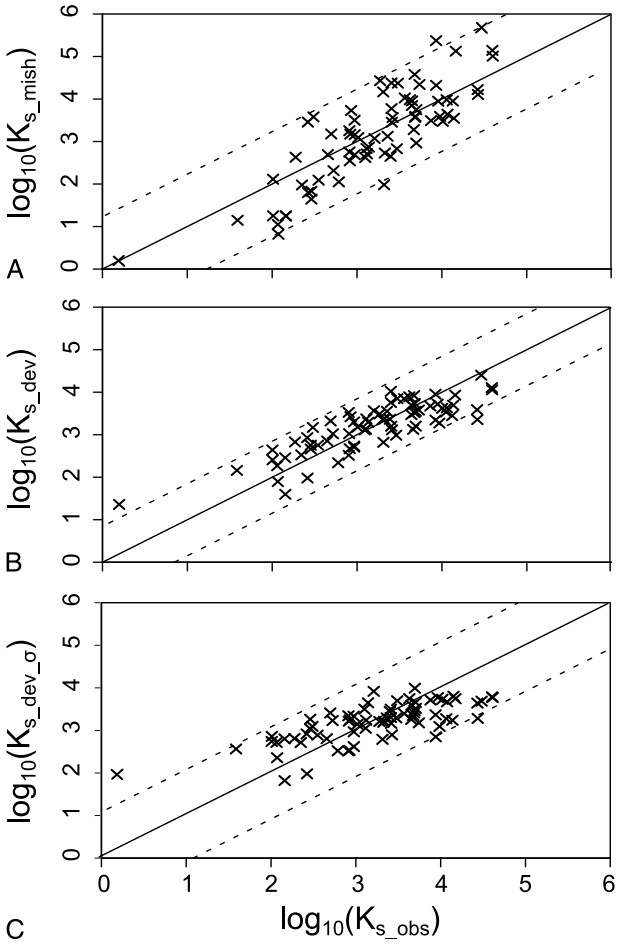

FIG. 3. Uncertainty bands related to the 95% CI for (A) the K_{s_mish}, (B) the proposed K_{s_dev}, and (C) the $K_{s\_dev\_\sigma}$ models.

into K_{s_dev} ($K_{s\_dev\_\sigma}$; Eq.(19)), which reduces one degree of freedom, would have drastically deteriorated the predictions. Nonetheless, Fig. 3B, C shows that K_{s_dev} and $K_{s\_dev\_\sigma}$ are well aligned to the line 1:1, defining a "cloud of points" within the confidence intervals (described later), with less than two outliers. The proposed implementation of σ_p into the K_s model can be considered as efficient because $K_{s\_dev\_\sigma}$ leads to a reduction of the degree of freedom without reducing significantly the accuracy of the model.

Analysis of residuals with regard to the predictions assists in detecting model structural errors. Good models must ensure that the residuals have no correlation with either observed or predicted values. The residuals of the K_s models are computed as follows:

$$E_r = \log_{10} K_{s\_p} - \log K_{s\_obs} \quad (24)$$

where K_{s_p} and K_{s_obs} are predicted and observed values, respectively. For the K_{s_mish}, K_{s_dev}, $K_{s\_dev\_\sigma}$ models, E_r is plotted versus predicted values in Fig. 4B, D, F, respectively. All the developed models, except K_{s_mish} model, show clearly that E_r and the predicted values are uncorrelated, which suggests that the developed models contain no evident structural errors. In contrast, K_{s_mish} exhibits a clear linear dependency of E_r with predicted values with an underestimation for low hydraulic conductivities and an overestimation of high hydraulic conductivities (Fig. 4B). This clearly demonstrates the inadequacy of K_{s_mish} in comparison with K_{s_dev}, $K_{s\_dev\_\sigma}$. This may be because K_{s_mish} lacks degree of freedom compared with the other models.

The probability plots of E_r show normal distribution (Fig. 4A, C, E). This is confirmed by the KST (in Table 8) that show that the critical probabilities are higher than the threshold of 5%. Furthermore, the residual E_r are centered, with means close to zero (Mean in Table 8). Clearly, the three models obey a lognormal distribution. Therefore, the 95% confidence intervals for the K_s models (95% CI), which define the uncertainty bands of the models, are computed as approximately twice the S.D. and depicted in Fig. 3A to C. Values for S.D. and 95% CI are detailed in Table 8 and show K_{s_dev} (95% CI $10^{\pm 0.85}$) < $K_{s\_dev\_\sigma}$ (95% CI $10^{\pm 1.08}$) < K_{s_mish} (95% CI $10^{\pm 1.23}$). Thus, the range of confidence intervals of K_{s_dev} and $K_{s\_dev\_\sigma}$ lies well within the ranges of the uncertainties related to K_s measurement methods from the field/laboratory that are in the order of $\log_{10} K_s \pm 10^{1.8}$ cm d^{-1}. In contrast, for K_{s_mish}, 95% CI is wider, leading to a less accurate prediction of saturated hydraulic conductivity (Fig. 4A).

Thus, when performing inverse modeling, the minimum and maximum values of K_{s_dev}, summarized in Table 10, depend on the value of θ_r, θ_s, h_m, and σ and on 95% CI of the K_{s_dev}, which is $10^{\pm 0.85}$. To visualize the reduction of the feasible parameter space (Table 5), we plot in Fig. 5 the feasible parameter space of K_s, which is in between the upper and lower limits of $10^{\pm 1.08}$ $K_{s\_dev\_\sigma}$. Figure 5 clearly shows that the usage of $K_{s\_dev\_\sigma}$ reduces dramatically the feasible parameter space of K_s.

TABLE 8. Optimal Parameters of the Saturated Hydraulic Conductivity Models Described in Table 1

	K_{s_dev}	K_{s_mish}	$K_{s\_dev\_\sigma}$
τ_1	0.761	1.083	0.761
τ_2	1.022	2.000	1.022
τ_3	5.072	2.500	5.072
$P_{\sigma 1}$	—	—	0.592
$P_{\sigma 2}$	—	—	0.768
NSE	0.71	0.39	0.53
RMSE	0.42	0.61	0.54
R^2	0.71	0.39	0.53
Bias	0.35	0.50	0.43
Mean	$5.86\ 10^{-12}$	$-2.26\ 10^{-12}$	$1.82\ 10^{-12}$
σ_e	0.42	0.62	0.54
95% CI	±0.85	±1.23	±1.08
KST	0.68	0.77	0.82
Outliers	2	2	2

The statistical information of the different models is provided for $\log_{10} K_s$. Where NSE is the Nash-Sutcliffe (1970) efficiency coefficient; RMSE is the root mean square error; R^2 is the coefficient of determination; Outliers are the number of data points that differ significantly from model predictions. The following statistics are based on the modeled residuals (E_r) computed as the differences between predicted data and observations: KST is the critical probability for Kolmogorov-Smirnov tests of normality; σ_e is the S.D.; 95% CI is the 95% confidence interval by assuming that the errors are lognormal distributed. The optimal parameters are well within the feasible range described in Table 2.

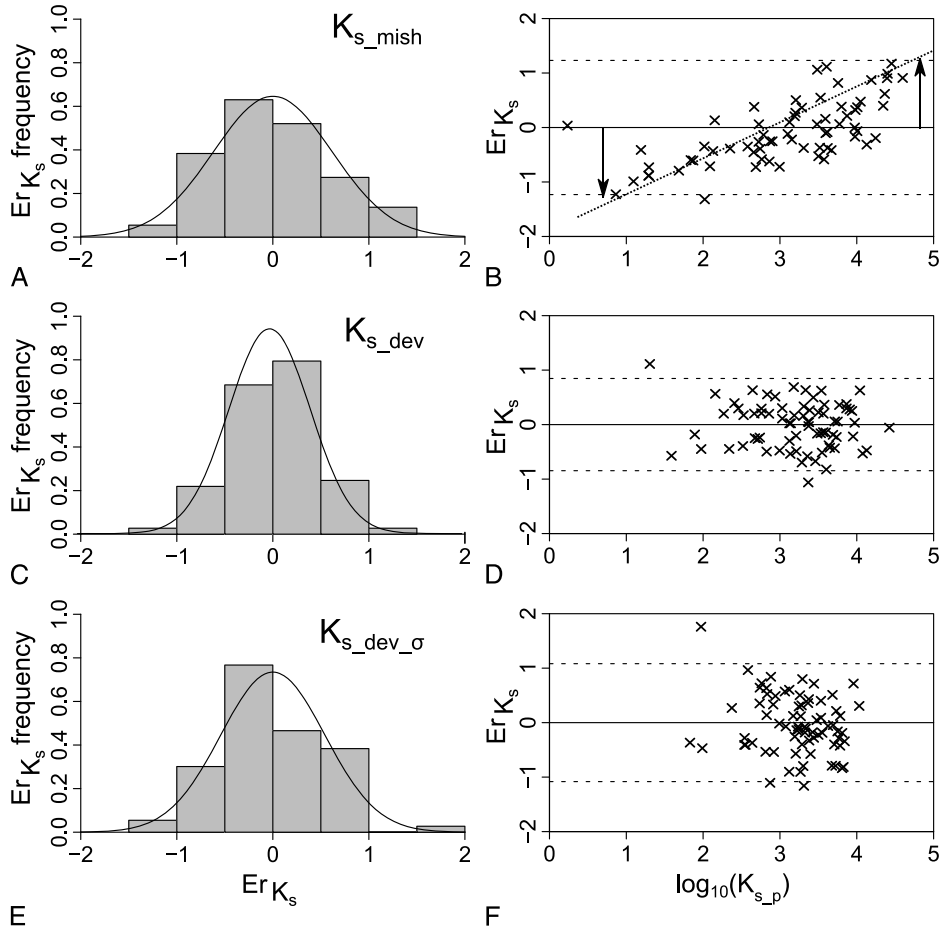

FIG. 4. A, C, E, Residual distributions (bars), along with normal distributions (lines). B, D, F, Residuals versus predicted values. Cases of Mish Model (A, B) and the proposed K_{s_dev} (C, D) and $K_{s\_dev\_\sigma}$ (E, F). models.

Sensitivity Analysis and Physical Interpretation of the Tortuosity Parameters of the Developed K_s Model

To establish if K_{s_dev} is not overparameterized and to determine the sensitivity of τ_1, τ_2, τ_3, we carried out a sensitivity analysis described in Table 9. In the sensitivity analysis, one parameter is "removed" in turns and the remaining two parameters are optimized. The sensitivity of the parameters is proportional to how much the results deteriorate (detailed in difference in accuracy Δ) when the parameter in question is not used compared with optimizing all the parameters (Step A of Table 9).

The results shown in Table 9 suggest that τ_1, τ_2, τ_3 are highly sensitive ($\Delta NSE_{log10} \leq -0.2$) especially for the tortuosity factor τ_2 of Fatt and Dykstra (1951), with $\Delta NSE_{log10} \leq -3.8$ and not τ_1, as it may be expected, which corrects for the slope of the curve. Table 9 suggests that the most sensitive parameters in increasing order are τ_2 followed by τ_1 and τ_3. Thus, further simplification of the model would considerably deteriorate the predictability of the K_{s_dev}.

These results shed light to why K_{s_mish} gives poorer results compared with K_{s_dev}. This is because K_{s_mish} has only one degree of freedom, which is τ_1. Nevertheless, this study shows that τ_2 is a more sensitive parameter. Furthermore, this explains why there is a linear correlation between E_r and K_{s_mish}, which shows that K_{s_mish} structure is not wrong but that K_{s_mish} is underparameterized.

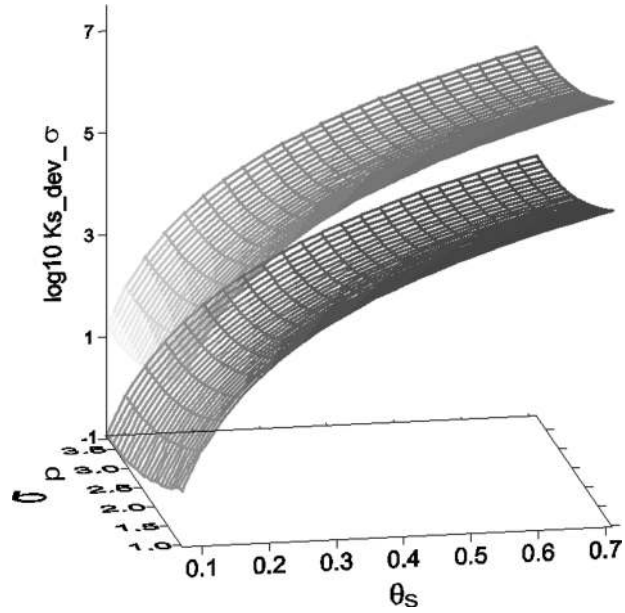

FIG. 5. Three-dimensional plot showing that the feasible range of K_s is in-between the lower and upper limits of $K_{s\_dev\_\sigma}$, which depends on the values of θ_s and σ_p.

TABLE 9. Sensitivity Analysis of the Parameters τ_1, τ_2, and τ_3 of K_{s_dev} by Determining the Decrease of Accuracy (Δ) When the Parameter in Question Is Not Used Compared With **A** Where All the Parameters Are Optimized

	τ_1	τ_2	τ_3	NSE_{log10}	$RMSE_{log10}$	$Bias_{log10}$	Δ NSE_{log10}	Δ $RMSE_{log10}$	Δ $Bias_{log10}$
A	0.761	1.022	5.072	0.71	0.42	0.35	—	—	—
B	1.00	0.983	7.177	0.47	0.57	0.47	−0.24	−0.15	−0.11
C	0.464	2.00	1.01	−4.53	1.85	1.35	−3.82	−1.43	−1.05
D	0.549	1.201	1.00	0.50	0.56	0.45	−0.21	−0.14	−0.11

Where NSE is the Nash-Sutcliffe (1970) efficiency and RMSE is the root mean square error.

The results show that the most sensitive parameters in the increasing order is τ_2, followed by τ_1 and τ_3.

Table 8 shows that for K_{s_dev}, $K_{s\_dev\_\sigma}$ the tortuosity parameters τ_1, τ_2, τ_3 are well within the physical limits recorded in Table 2. Therefore, this study complies with that of Fatt and Dykstra (1951), which states that liquid flowing in the crevices and small pores will travel a more tortuous path than liquid flowing through the large pores. Our results are also in agreement with those of Vervoort and Cattle (2003), which state that, in high-porosity media, the large effective pores tend to be more connected than the smaller effective pores. Thus, we can attribute a physical interpretation to the τ_1, τ_2, τ_3 parameters.

CONCLUSIONS

An increasingly attractive cost-efficient alternative is to derive the effective hydraulic parameters by inverting the Richards equation that governs water flow in unsaturated soil. Nevertheless, relatively large uncertainties can occur when predicting water fluxes because of nonuniqueness of the inverted hydraulic parameters. We proposed an algorithm to reduce the nonuniqueness of the inverted hydraulic parameters.

Traditionally, the minimum and maximum ranges for each individual parameter are provided before an inverse modeling exercise (e.g., Table 4). Nevertheless, this traditional method has the disadvantage that it includes nonphysical parameter combination sets. We therefore propose methods to narrow down the feasible range by developing algorithms to preclude nonphysical combinations of hydraulic parameters.

We selected the Kosugi model, which describes the water retention and the hydraulic conductivity relationships, because there is a negative linear correlation between two of its parameters (h_m and σ), and therefore, enabling it to reduce the feasible parameter space. To further reduce the feasible parameter space, we developed two physically based models to predict saturated hydraulic conductivity from four or three parameters describing the Kosugi characteristic curve.

The proposed saturated hydraulic conductivity model is developed by modifying the approach of Childs and Collis-George (1950) by estimating the soil water flux through a continuous function of the pore-size distribution of Kosugi (1996). We combined the Hagen-Poiseuille equation with the Darcy law and introduced constant empirical universal tortuosity parameters of Fatt and Dykstra (1951) and incorporated another tortuosity parameter to take into account that high-porosity media tend to be more connected and should have a lower tortuosity (Vervoort and Cattle, 2003). The Kosugi soil hydraulic parameters were calibrated by selecting 73 water

TABLE 10. Summary of the Feasible Parameter Space of the Kosugi Hydraulic Parameters That Is Reduced Dynamically for σ and K_s, Where $C = 1.03663 \times 10^9$ cm d^{-1}

Minimum	θ_s	$m^3\ m^{-3}$	0.32
	θ_r	$m^3\ m^{-3}$	0.00
	h_m	cm	17
	σ_p	cm	$0.592\ (Ln\ h_m - 1)^{0.7679} - 0.89$
	K_{s_dev}	cm d^{-1}	$\dfrac{0.761\ C\ (\theta_s-\theta_r)^{5.072}\ \left(\frac{0.149}{h_m}\right)^{1.022}\ \int_0^1 \left\{\dfrac{1}{\exp\left[erfc^{-1}(2\ S_e)\ \sigma\sqrt{2}\right]}\right\}^{1.022} dS_e}{10^{0.85}}$
Maximum	θ_s	$m^3\ m^{-3}$	0.71
	θ_r	$m^3\ m^{-3}$	0.25
	h_m	cm	$2.57\ 10^5$
	σ_p	cm	$0.592\ (Ln\ h_m - 1)^{0.7679} + 0.89$
	K_{s_dev}	cm d^{-1}	$0.761\ C\ (\theta_s-\theta_r)^{5.072}\ \left(\frac{0.149}{h_m}\right)^{1.022}\ \int_0^1 \left\{\dfrac{1}{\exp\left[erfc^{-1}(2\ S_e)\ \sigma\sqrt{2}\right]}\right\}^{1.022} dS_e\ 10^{0.85}$

The feasible range of θ_s, θ_r, and h_m is obtained from Table 5.

retention and unsaturated curves data sets from the UNSODA and HYPRES database, which also contain measured saturated hydraulic conductivity and saturated soil moisture.

The developed saturated hydraulic conductivity model (K_{s_dev}) has shown good performance with an NSE of 0.71. Because no correlation was obtained between residuals and observed saturated hydraulic conductivity, we suggest that the developed model has no obvious structural errors. A sensitivity analysis was performed with the three fitting tortuosity parameters, and it was found that all the parameters are necessary to give good performance and their optimal values were found to comply with the soil physics theory. The developed saturated hydraulic conductivity model errors were found to be log-normally distributed, with the 95% CI of K_s being $\pm 1 \times 10^{0.85}$ cm d^{-1}, which is in the same order of magnitude of field and/or laboratory K_s measurements. The proposed saturated hydraulic conductivity model was compared with the modified saturated hydraulic conductivity of Mishra and Parker (1990) model (K_{s_mish}), such that it uses the Kosugi (1996) parameters instead of the van Genuchten (1980) hydraulic parameters. We found that the developed saturated hydraulic conductivity model outperforms K_{s_mish}.

To further reduce the nonuniqueness, we built a second model ($K_{s\_dev\_\sigma}$), which exploits the correlation between $\log_{10} h_m$ and σ and found a reasonable relationship. We introduced the σ model into the saturated hydraulic conductivity models, K_{s_dev}, and found that it leads to estimate quasi as good as the original model. The proposed $K_{s\_dev\_\sigma}$ can be considered parsimonious because it leads to a reduction of the degree of freedom without reducing significantly the accuracy of the model. A summary of the developed model with the dynamic feasible range of its parameters is provided in Table 10.

The reduction in uncertainties of the forwarded water flux by using the proposed methodology of restraining the feasible parameter space dynamically, summarized in Table 1, should be assessed. Without considering the scale issues, this can be performed with precise weighing lysimeters for which the storage and water fluxes are measured (e.g., drainage and evapotranspiration) (e.g., Abbaspour et al., 1999; Kosugi and Katsuyama, 2001, 2004; Scanlon et al., 2005; Durner et al., 2008). Different experiments should be performed under contrasting hydroclimate conditions because Pollacco and Mohanty (2012) showed that the sensitivity of hydrological parameters is highly dependent on the hydroclimate.

ACKNOWLEDGMENTS

We acknowledge the partial support of National Science Foundation (CMG/DMS Grant No. 0934837) and NASA THPs (NNX09AK73G) grants. We also thank Lilly A. (Macaulay Land Use Research Institute) for entrusting us with the HYPRES data set. We thank J. Vrugt for having provided the global optimization code AMALGAM and assisted us in its implementation.

ABBREVIATIONS

θ: soil moisture; $\theta(h)$: soil water retention functions; $K(\theta)$: hydraulic conductivity functions; K_{s_dev}: developed saturated hydraulic conductivity model that predicts K_s from four Kosugi parameters (θ_r, θ_r, h_m, and σ); $K_{s\_dev\_\sigma}$: proposed model that predicts K_s from 3 Kosugi parameters (θ_s, θ_r and h_m); K_{s_mish}: modified model of Mishra and Parker (1990) that predicts K_s from 4 Kosugi parameters (θ_s, θ_r, h_m and σ); **OF:** objective function; $\mathbf{OF_{ks}}$: objective function of the fitted parameters of the K_s models; $\mathbf{OF}_\sigma$: objective function of the fitted parameters of the σ models; **WOF:** weighted objective function σ_p: predicts σ from h_m Kosugi parameter.

ABBREVIATIONS

Variables and symbols used in the study:

σ: S.D. of log-transformed matric potential head (-);

σ_p: predicted value for σ (-);

θ: soil water content (L L^3);

θ_r: residual water content (L L^3);

θ_s: saturated water content (L L^3);

A: unit cross-sectional area (L^2);

H: total hydraulic head (L);

h: soil matric potential head (L);

h_m : median soil matric potential head (L);

K: soil hydraulic conductivity (L T^{-1});

K_r: relative hydraulic conductivity (-);

K_s: saturated hydraulic conductivity (L T^{-1});

K_{s_dev}: developed model that predicts K_s from θ_r, θ_r, h_m, and σ;

$K_{s\_dev\_\sigma}$: proposed model that predicts K_s from θ_s, θ_r, and h_m;

K_{s_mish}: modified model of Mishra and Parker (1990) that predicts K_s from θ_s, θ_r, h_m, and σ;

K_{s_obs}: observed value for K_s (-);

L: path length in the direction of the flow (L);

τ_1: macroscopic tortuosity-connectivity parameter (L L^{-1});

τ_2: microscopic tortuosity-connectivity parameter to adjusts the shape of the capillary tube (-);

τ_3: pore-connectivity parameter (-);

R: pore-radius (L);

R_m: pore radius distribution parameter (L);

S_e: degree of saturation (-);

Y: Young-Laplace constant of the capillary equation (L^2);

q: water flux (L T^{-1});

Q: water volumetric flow rate (L^3 T^{-1});

C: constant in the Poiseuille equation 1.03663×10^9 cm d^{-1};

$P_{\sigma 1}$: first fitting parameter of Eq.(18) (-);

$P_{\sigma 2}$: second fitting parameter of Eq.(18) (-);

ϕ: soil porosity (L^3 L^{-3})

REFERENCES

Abbaspour K. C., M. A. Sonnleitner, and R. Schulin. 1999. Uncertainty in estimation of soil hydraulic parameters by inverse modeling: Example lysimeter experiments. Soil Sci. Soc. Am. J. 63:501–509.

Bear J. 1972. Dynamics of Fluids in Porous Media. Elsevier, New York

Beydoun H., and F. Lehmann. 2006. Drainage experiments and parameter estimation in unsaturated porous media (Expériences de drainage et estimation de paramètres en milieu poreux non saturé). Comptes Rendus Geosci. 338:180–187.

Binley A., and K. Beven. 2003. Vadose zone flow model uncertainty as conditioned on geophysical data. Ground Water. 41:119–127.

Bormann H., and K. Klaassen. 2008. Seasonal and land use dependent variability of soil hydraulic and soil hydrological properties of two Northern German soils. Geoderma. 145:295–302.

Brooks R. H., and A. T. Corey. 1964. Hydraulic properties of porous media. Hydrol. Pap. 3. Colorado State University, Ft Collins.

Cannavo P., L. Vidal-Beaudet, B. Béchet, L. Lassabatère, and S. Charpentier. 2010. Spatial distribution of sediments and transfer properties in soils in a stormwater infiltration basin. J. Soils Sediments. 10:1499–1509.

Childs E. C., and N. Collis-George. 1950. The permeability of porous materials. Proc. R. Soc. Lon. Ser. A. 201:392–405.

Corey A. T. 1979. Mechanics of Heterogeneous Fluids in Porous Media. Water Resources Publications, Littleton, CO.

Darcy H. 1856. Les fontaines publiques de la ville de Dijon. Dalmont, Paris, France.

Das N. N., and B. P. Mohanty. 2006. Root zone soil moisture assessment using remote sensing and vadose zone modeling. Vadose Zone J. 5:296–307.

Das N. N., B. P. Mohanty, M. H. Cosh, and T. J. Jackson. 2008. Modeling and assimilation of root zone soil moisture using remote sensing observations in Walnut Gulch Watershed during SMEX04. Remote Sensing Environ. 112:415–429.

Das Gupta S., B. P. Mohanty, and J. M. Kohne. 2006. Soil hydraulic conductivities and their spatial and temporal variations in a vertisol. Soil Sci. Soc. Am. J. 70:1872–1881.

Durner W., U. Jansen, and S. C. Iden. 2008. Effective hydraulic properties of layered soils at the lysimeter scale determined by inverse modelling. Eur. J. Soil Sci. 59:114–124.

Fatt I., and H. Dykstra. 1951. Relative permeability studies. T. Am. I. Min. Met. Eng. 192:249–256.

Fodor N., R. Sandor, T. Orfanus, L. Lichner, and K. Rajkai. 2011. Evaluation method dependency of measured saturated hydraulic conductivity. Geoderma. 165:60–68.

Guarracino L. 2007. Estimation of saturated hydraulic conductivity Ks from the van Genuchten shape parameter. Water Resources Res. 43.

Han H., D. Gimenez, and A. Lilly. 2008. Textural averages of saturated soil hydraulic conductivity predicted from water retention data. Geoderma. 146:121–128.

Hayashi Y., K. Ken'ichirou, and T. Mizuyama. 2006. Changes in pore size distribution and hydraulic properties of forest soil resulting from structural development. J. Hydrol. 331:85–102.

Ines A. V. M., and P. Droogers. 2002. Inverse modeling in estimating soil hydraulic functions: A genetic algorithm approach. Hydrol. Earth Syst. Sci. 6:49–65.

Ines A. V. M., and B. P. Mohanty. 2008a. Near-surface soil moisture assimilation for quantifying effective soil hydraulic properties under different hydroclimatic conditions. Vadose Zone J. 7:39–52.

Ines A. V. M., and B. P. Mohanty. 2008b. Near-surface soil moisture assimilation for quantifying effective soil hydraulic properties using genetic algorithm: 1. Conceptual modeling. Water Resources Res. 44. doi:Artn W06422.

Ines A. V. M., and B. P. Mohanty. 2008c. Parameter conditioning with a noisy Monte Carlo genetic algorithm for estimating effective soil hydraulic properties from space. Water Resources Res. 44. doi:Artn W08441.

Jhorar R. K., W. G. M. Bastiaanssen, R. A. Feddes, and J. C. Van Dam. 2002. Inversely estimating soil hydraulic functions using evapotranspiration fluxes. J. Hydrol. 258:198–213.

Kabat P., R. W. A. Hutjes, and R. A. Feddes. 1997. The scaling characteristics of soil parameters: From plot scale heterogeneity to subgrid parameterization. J. Hydrol. 190:363–396.

Kosugi K. 1994. Three-parameter lognormal distribution model for soil water retention. Water Resources Res. 30:891–901.

Kosugi K. 1996. Lognormal distribution model for unsaturated soil hydraulic properties. Water Resources Res. 32:2697–2703.

Kosugi K., J. W. Hopmans, and J. H. Dane. 2002. Water retention and storage—Parametric models. *In*: Methods of Soil Analysis. Part 4. Physical Methods. E. J. H. Dane and G. C. Topp (eds.). Soil Science Society of America, Madison, Wisc pp. 739–758.

Kosugi K., and M. Katsuyama. 2001. Measurements of groundwater recharge rate and unsaturated convective chemical fluxes by suction controlled lysimeter. Impact of human activity on groundwater dynamics. Proceedings of the 6th IAHS Scientific Assembly, Maastricht, Netherlands, 18-27 July 2001, pp. 19–24.

Kosugi K., and M. Katsuyama. 2004. Controlled-suction period lysimeter for measuring vertical water flux and convective chemical fluxes. Soil Sci. Soc. Am. J. 68:371–382.

Lassabatere L., R. Angulo-Jaramillo, D. Goutaland, L. Letellier, J. P. Gaudet, and T. Winiarski, et al 2010. Effect of the settlement of sediments on water infiltration in two urban infiltration basins. Geoderma. 156:316–325.

Lassabatere L., R. Angulo-Jaramillo, J. M. Soria-Ugalde, J. Šimůnek, and R. Haverkamp. 2009. Numerical evaluation of a set of analytical infiltration equations. Water Resources Res. 45: W12415.

Lassabatere L., R. Angulo-Jaramillo, J. M. Soria Ugalde, R. Cuenca, I. Braud, and R. Haverkamp. 2006. Beerkan estimation of soil transfer parameters through infiltration experiments—BEST. Soil Sci. Soc. Am. J. 70:521–532.

Leij F. J., W. J. Alves, M. T. Van Genuchten, and J. R. Williams. 1999. The UNSODA unsaturated soil hydraulic database. Proceedings of the International Workshop on Characterization and Measurement of the Hydraulic Properties of Unsaturated Porous Media. Riverside, Calif, 1269–1281.

Lilly A., A. Nemes, W. J. Rawls, and Y. A. Pachepsky. 2008. Probabilistic approach to the identification of input variables to estimate hydraulic conductivity. Soil Sci. Soc. Am. J. 72:16–24.

Mallants D., D. Jacques, P. -H. Tseng, M. T. van Genuchten, and J. Feyen. 1997. Comparison of three hydraulic property measurement methods. J. Hydrol. 199:295–318.

Messing I. 1989. Estimation of the saturated hydraulic conductivity in clay soils from soil-moisture retention data. Soil Sci. Soc. Am. J.. 53:665–668.

Minasny B., and D. J. Field. 2005. Estimating soil hydraulic properties and their uncertainty: The use of stochastic simulation in the inverse modeling of the evaporation method. Geoderma. 126:277–290.

Mishra S., and J. C. Parker. 1990. On the relation between saturated conductivity and capillary retention characteristics. Ground Water. 28:775–777.

Mohanty B. P., M. D. Ankeny, R. Horton, and R. S. Kanwar. 1994a. Spatial analysis of hydraulic conductivity measured using disc infiltrometers. Water Resources Res. 30:2489–2498.

Mohanty B. P., R. S. Kanwar, and C. J. Everts. 1994b. Comparison of saturated hydraulic conductivity measurement methods for a glacial till soil. Soil Sci. Soc. Am. J. 58(3):672–677.

Mohanty B. P., and J. T. Zhu. 2007. Effective hydraulic parameters in horizontally and vertically heterogeneous soils for steady-state land-atmosphere interaction. J. Hydrometeorol. 8:715–729.

Mualem Y. 1976. New model for predicting the hydraulic conductivity of unsaturated porous media. Water Resources Res. 12:513–522.

Mualem Y., and G. Dagan. 1978. Hydraulic conductivity of soils: unified approach to the statistical models. Soil Sci. Soc. Am. J.. 42:392–395.

Nash J. E., and J. V. Sutcliffe. 1970. River flow forecasting through conceptual models part I - A discussion of principles. J. Hydrol. 10:282–290.

Nasta P., L. Lassabatere, M. M. Kandelous, J. Šimunek, and R. Angulo-Jaramillo. 2012. Analysis of the role of tortuosity and infiltration constants in the Beerkan method. Soil Sci. Soc. Am. J. 76:1999–2005.

Peters A., W. Durner, and G. Wessolek. 2011. Consistent parameter constraints for soil hydraulic functions. Adv. Water Res. 34:1352–1365.

Pollacco J. A. P. 2005. Inverse Methods to Determine Parameters in a Physically Based Model of Soil-Water Balance. University of Newcastle upon Tyne, Newcastle upon Tyne, UK.

Pollacco J. A. P., and B. P. Mohanty. 2012. Uncertainties of water fluxes in soil-vegetation-atmosphere transfer models: Inverting surface soil moisture and evapotranspiration retrieved from remote sensing. Vadose Zone J. 11:11.

Pollacco J. A. P., J. M. S. Ugalde, R. Angulo-Jaramillo, I. Braud, and B. Saugier. 2008. A Linking Test to reduce the number of hydraulic parameters necessary to simulate groundwater recharge in unsaturated soils. Adv. Water Res. 31:355–369.

Ritter A., F. Hupet, R. Muñoz-Carpena, S. Lambot, and M. Vanclooster. 2003. Using inverse methods for estimating soil hydraulic properties from field data as an alternative to direct methods. Agric. Water Manage. 59:77–96.

Romano N. 1993. Use of an inverse method and geostatistics to estimate soil hydraulic conductivity for spatial variability analysis. Geoderma. 60:169–186.

Romano N., and A. Santini. 1999. Determining soil hydraulic functions from evaporation experiments by a parameter estimation approach: Experimental verifications and numerical studies. Water Resources Res. 35:3343–3359.

Scanlon B. R., D. G. Levitt, R. C. Reedy, K. E. Keese, and M. J. Sully. 2005. Ecological controls on water-cycle response to climate variability in deserts. Proc. Natl. Acad. Sci. U. S. A. 102:6033–6038.

Schaap M. G., and M. T. van Genuchten. 2006. A modified Mualem–van Genuchten formulation for improved description of the hydraulic conductivity near saturation. Vadose Zone J. 5:27–34.

Scharnagl B., J. A. Vrugt, H. Vereecken, and M. Herbst. 2011. Inverse modeling of *in situ* soil water dynamics: Investigating the effect of different prior distributions of the soil hydraulic parameters. Hydrol. Earth Syst. Sci. 15:3043–3059.

Shin Y., B. P. Mohanty, and A. V. M. Ines. 2012. Soil hydraulic properties in one-dimensional layered soil profile using layer-specific soil moisture assimilation scheme. Water Resources Res. 48.

Sobieraj J. A., H. Elsenbeer, and G. Cameron. 2004. Scale dependency in spatial patterns of saturated hydraulic conductivity. Catena. 55:49–77.

Sonnleitner M. A., K. C. Abbaspour, and R. Schulin. 2003. Hydraulic and transport properties of the plant-soil system estimated by inverse modelling. Eur. J. Soil Sci. 54:127–138.

Suwardji P., and P. L. Eberbach. 1998. Seasonal changes of physical properties of an Oxic Paleustalf (Red Kandosol) after 16 years of direct drilling or conventional cultivation. Soil Till. Res. 49:65–77.

ter Braak C. J. F., and J. A. Vrugt. 2008. Differential evolution Markov chain with snooker updater and fewer chains. Stat. Comput. 4:435–446.

Tyler S. W., and S. W. Wheatcraft. 1990. Fractal processes in soil-water retention. Water Resources Res. 26:1047–1054.

Upchurch D. R., L. P. Wilding, and J. L. Hartfield. 1988. Methods to evaluate spatial variability. *In*: Reclamation of Disturbed Lands L. R. Hossner (ed.). CRC Press, Boca Raton, FL, pp. 201–229.

van Genuchten M. T. 1980. Closed-form equation for predicting the hydraulic conductivity of unsaturated soils. Soil Sci. Soc. Am. J. 44:892–898.

Van Genuchten M. T., F. J. Leij, and S. R. Yates. 1991. The RETC code for quantifying the hydraulic functions of unsaturated soils. EPA Rep. 600/2-91/065, U.S. Salinity Laboratory, USDA-ARS, Riverside, Calif.

Vervoort R. W., and S. R. Cattle. 2003. Linking hydraulic conductivity and tortuosity parameters to pore space geometry and pore-size distribution. J. Hydrol. 272:36–49.

Vrugt J. A., P. H. Stauffer, T. Wohling, B. A. Robinson, and V. V. Vesselinov. 2008. Inverse modeling of subsurface flow and transport properties: A review with new developments. Vadose Zone J. 7:843–864.

Vrugt J. A., and C. J. F. ter Braak. Differential evolution adaptive differential evolution adaptive metropolis with sampling from the past and subspace updating. SIAM J. Optimization. In press.

Wollschläger U., T. Pfaff, and K. Roth. 2009. Field scale effective hydraulic parameterisation obtained from TDR time series and inverse modeling. Hydrol. Earth Syst. Sci. Discuss. 6:1489–1522.

Wösten J. H. M., A. Lilly, A. Nemes, and C. Le Bas. 1998. Final Report on the EU-Funded Project Using Existing Soil Data to Derive Hydraulic Parameters for Simulation Models in Environmental Studies and in Land Use Planning. DLO Winand Staring Centre, Wageningen, The Netherlands.

Wösten J. H. M., A. Lilly, A. Nemes, and C. Le Bas. 1999. Development and use of a database of hydraulic properties of European soils. Geoderma. 90:169–185.

Yilmaz D., L. Lassabatere, R. Angulo-Jaramillo, D. Deneele, and M. Legret. 2010. Hydrodynamic characterization of basic oxygen furnace slag through an adapted best method. Vadose Zone J. 9:107–116.

Yilmaz D., L. Lassabatere, D. Deneele, R. Angulo, and M. Legret. 2013. Influence of carbonation on the microstructure and the hydraulic properties of a basic oxygen furnace slag. Vadose Zone J. In press.

Yu B., J. Li, Z. Li, and M. Zou. 2003. Permeabilities of unsaturated fractal porous media. Int. J. Multiphase Flow. 29:1625–1642.